

# Fair free-form surfaces that are almost everywhere parametrically $C^2$

Kęstutis Karčiauskas, Jörg Peters

## Abstract

Compared to  $G^k$  continuity,  $C^k$  continuity simplifies the construction of functions on surfaces and their refinement, e.g. to solve differential equations on the surface. The new class of almost everywhere parametrically  $C^2$  free-form surfaces provide such a parameterization. For example, a new bi-6 construction combines a fast-contracting  $C^2$  guided subdivision surface with a tiny multi-sided  $G^1$  cap. The cap is chosen to be smaller than any refinement anticipated for geometric modeling or computing on surfaces. Fast contraction means that one subdivision step shrinks the remaining hole more than three steps of Catmull-Clark subdivision. This yields smooth surfaces consisting of a finite number of pieces that are suitable for engineering practice. Both the subdivision construction and the cap are guided by a reference surface. This guide conveys the basic shape, but has a different structure and lower smoothness.

## 1. Introduction

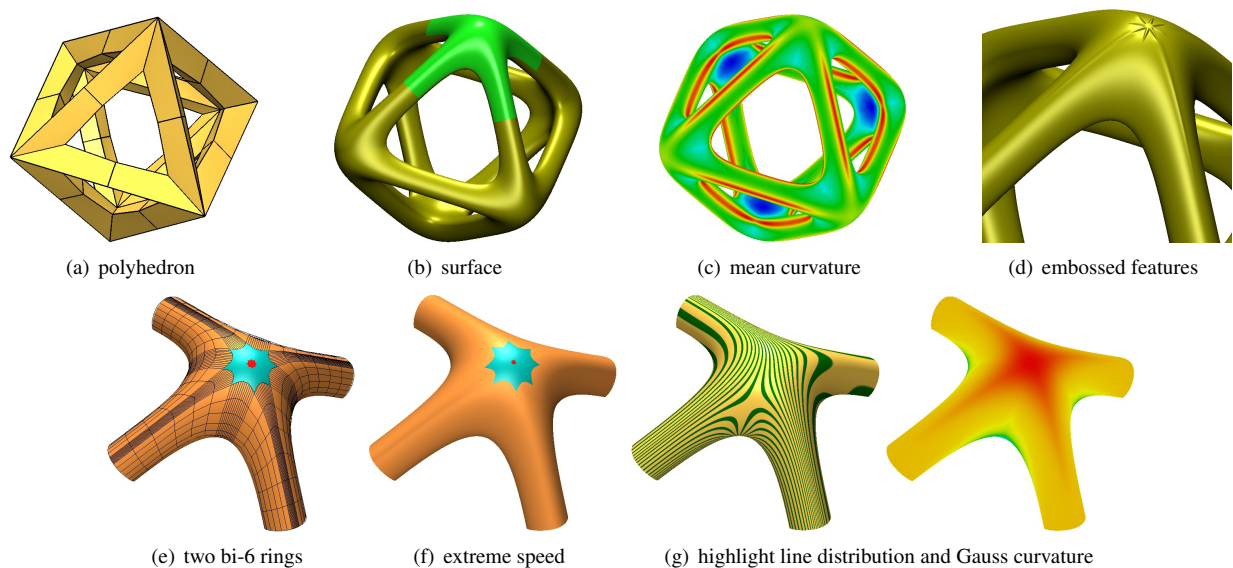


Figure 1: (a) An input mesh with no regular submesh for defining bi-3 tensor-product patches. The entire surface consists of multi-sided pieces. (b) One multi-sided piece, colored green. (c) The mean curvature distribution shows no variation except as forced by the macro-geometry. (d) Localized geometry modification illustrates refinability. (e) Two bi-6 rings plus red cap where only the first ring has its BB-net (Bézier control points) superimposed. (f) Yet faster choice of contraction. Both (e) and (f) result in visually identical highlight lines and Gauss curvature (g).

Relaxing parametric  $C^k$  to geometric  $G^k$  continuity in the construction of piecewise surfaces enables more flexible designs and shapes ([1, 2]). However, the change of parameter across the corresponding G-edges between patches complicates building and refining smooth functions on the union of the patches, e.g. texture maps or solutions of partial differential equations on the surface as domain [3, 4, 5, 6, 7]. Since smooth functions on a  $G^k$  surface need to have the same reparameterizations across G-edges as the surface itself [8] one needs to carefully keep the track of G-edges when refining G-functions. Moreover, the degrees of freedom arising from G-refinement on free-form

surfaces are irregularly distributed [9]. By contrast, where the reparameterizations are the identity or a binary split, i.e. across  $C^k$  edges, the proper refinement can be achieved by binary knot insertion without any bookkeeping other than the refinement level. Therefore the methods described in this paper seek to retain parametric continuity as much as possible by employing a new fast-contracting guided subdivision combined with a tiny cap. The fast-contracting subdivision generates a bi-6  $C^2$  surface that inherits its shape and good highlight line distribution from a guide surface. This fairer shape is the main distinguishing feature compared to Catmull-Clark subdivision, which is also almost everywhere parametrically  $C^2$  but has shape artifacts (see e.g. Fig. 12b). The final tiny  $G^1$  cap preserves the overall good highlight line distribution.

The input mesh Fig. 1a contains no  $4 \times 4$  submesh that could be interpreted as bicubic B-spline control points and admit standard spline refinement by knot insertion. Yet the new class of almost everywhere parametrically  $C^2$  free-form surfaces can not only smooth the genus 7 input, but can be refined to both support geometric detail and adaptive computing on the surface. Moreover, as illustrated in Fig. 1 e,f the speed of contraction of the bi-6 rings can be varied without immediate shape penalty.

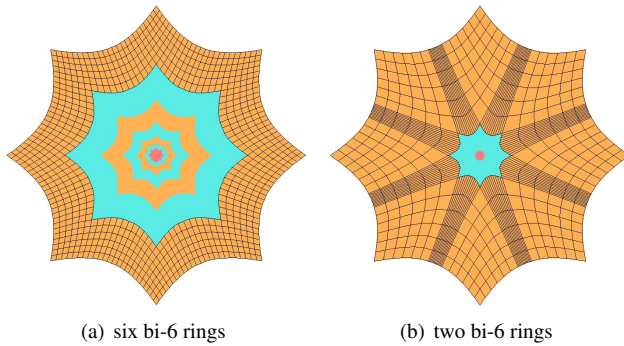


Figure 2: The contraction of (a) three steps at the speed of Catmull-Clark subdivision approximately equals that of (b) one bi-6 subdivision step. The (red) center is filled with a tiny  $G^1$  surface cap.

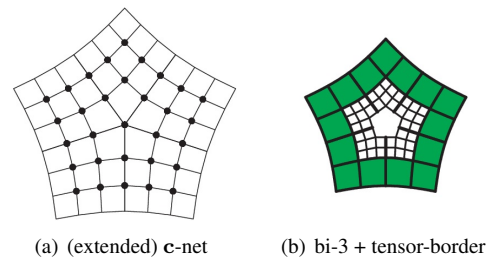


Figure 3: B-spline-like irregular control net and its tensor-border for  $n = 5$ . (a) The black bullets form the c-net. Together with the outermost layer of control points they form the *extended* c-net. Extended c-nets are used for examples since the bicubic ring provides a visual context for checking surface quality. (b) Schema of a bi-3 surface ring (green) and its tensor-border (mesh of BB-coefficients) of degree 3 and depth 2. The tensor-border is the input for the surface construction.

The new subdivision improves on the shape of early guided subdivision constructions such as [10], is easy to analyze and is  $C^2$  in the limit. For all practical purposes, see Fig. 2, it suffices to apply two steps of bi-6 subdivision and then fill the remainder with a tiny high quality bi-6  $G^1$  cap. The resulting surface

- consists of  $2 \times 3n$   $C^2$ -joined patches followed by  $n$  patches forming a tiny  $G^1$  cap;
- is  $C^2$  except for the tiny caps;
- is of degree bi-6 and
- provides surfaces with good highlight line distributions even for challenging input configurations.
- Functions on the surface are  $C^2$  refinable up to the level of the tiny cap.

*Overview.* Section 2 explains the input and the basic tools used for the construction such as the corner jet constructor. Section 2.3 defines the piecewise total degree 6 guide surface. Section 3 shows how sampling the composition of the guide with a characteristic parameterization results in bi-6 guided subdivision rings. Section 4 presents a full analysis of this subdivision including the proof of curvature continuity in the limit. For practical use, we suggest to only generate one or two subdivision rings and complete, see Section 5, the surface with a tiny cap (that does not negatively affect the shape). Section 6 illustrates the outcomes and discusses alternative construction choices, in particular the ‘speed sequence’ of the subdivision.

## 2. Definitions and Setup

### 2.1. A B-spline-like control net for irregular layout

The input is a network of quadrilateral facets, short quads. Nodes where four quads meet are regular, else *irregular*. We assume that each irregular node is surrounded by at least one layer of regular nodes. Fig. 3a shows the c-net (bullets) of an isolated node of valence  $n = 5$ . The c-net consists of the irregular node plus  $6n$  nodes forming two layers of quads surrounding it. Typically a third layer is added for evaluation of local shape (yielding the green surface in Fig. 3b). This allows assessing the highlight line distribution [11] across the transition which is as important as the internal quality of the cap.

Each  $4 \times 4$  sub-grid of nodes is interpreted as the B-spline control points of a bicubic tensor-product spline surface. Except at the irregular node, well-known formulas can be applied to convert the B-spline form to tensor-product Bernstein-Bézier form called *BB-form* in the following (see e.g. [1, 12]). The *tensor-product BB-form* of a polynomial of bi-degree  $d$  is

$$\mathbf{p}(u, v) := \sum_{i=0}^d \sum_{j=0}^d \mathbf{p}_{ij} B_i^d(u) B_j^d(v), \quad (u, v) \in \square := [0..1]^2, \quad B_k^d(t) := \binom{d}{k} (1-t)^{d-k} t^k$$

where  $B_k^d$  are the Bernstein polynomials of degree  $d$  and  $\mathbf{p}_{ij}$  are the *BB-coefficients*, so-named to distinguish from the *control points* of the B-spline form. Fig. 3b also shows the  $C^2$  prolongation of this surface ring, i.e. Hermite data represented as a grid (black) of bi-3 BB-coefficients. Specifically, the BB-coefficients  $\mathbf{p}_{ij}$ ,  $i = 0, \dots, 3$ ,  $j = 0, \dots, 2$ , represent Hermite data of order 2 along one boundary curve  $v = 0$ . When degree-raised to 5, we call these data  $\mathbf{t}_{CC}$ . More generally, in the remainder of this paper, we refer to second-order Hermite data of degree 5 along the loop of boundary curves as  $\mathbf{t}$ .

### 2.2. Corner jet constructors

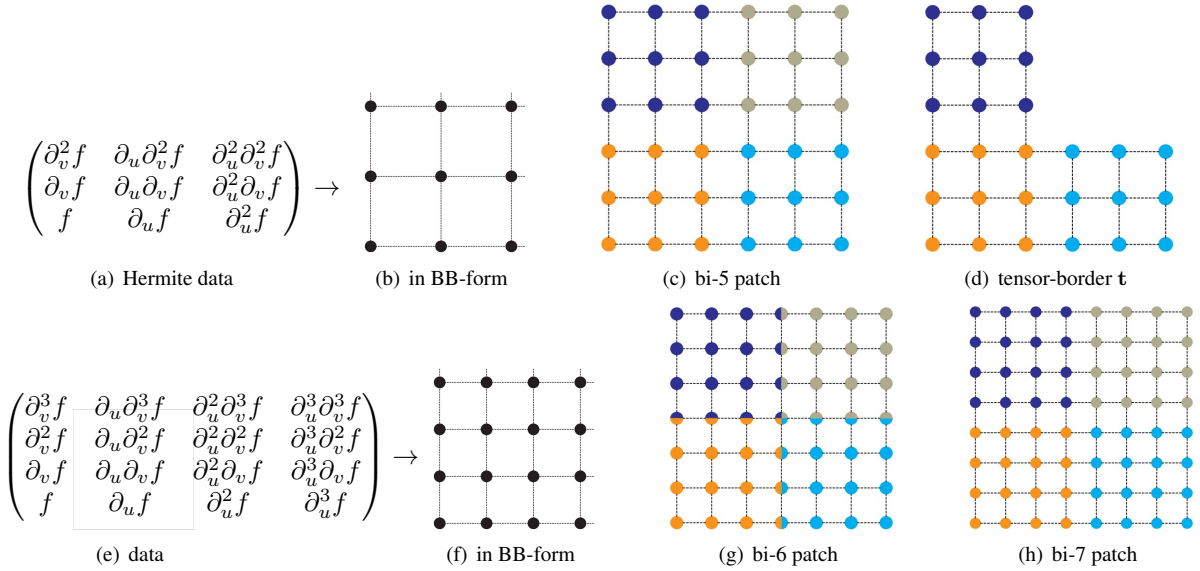


Figure 4: (a,e) Hermite data as partial derivatives converted to (b,f) BB-form; (c) a patch of degree bi-5; (d)  $L$ -shaped sector of the tensor-border  $\mathbf{t}$ .

We will construct the tensor-product patches and tensor-borders with a help of *corner jet constructors*  $[f]_{i \times i}^d$  that express, at a corner of domain square  $[0..1]^2$ , the expansion of a function  $f$  of order  $i - 1$  in either variable in BB-form of bi-degree  $d$ . For  $d = 5$  we use only  $i = 3$  (to construct the guide surface) hence for brevity denote this corner jet constructor as  $[f]^5$ . In the main construction  $d = 6$  and  $i = 4$  and the corner jet constructor is denoted by  $[f]^6$ .

Fig. 4c displays four corner jet constructors  $[f]^5$  merged to form a bi-5 patch while Fig. 4d illustrates the analogous assembly of an  $L$ -shaped sector of the tensor-border by applying a jet constructor at three corners. Fig. 4g displays four corner jet constructors  $[f]^6$  merged to form a bi-6 patch by averaging the overlapping BB-coefficients and Fig. 4h shows assembly of corner jets  $[f]^7$  into a bi-7 patch (that will be used for comparison with bi-6 surfaces.)

Several steps of the surface construction use a simple symmetric rule, called the C2-rule, illustrated in Fig. 5: two curve segments (of the same degree) in BB-form join  $C^2$  at their common end-point (marked as a big bullet) if and only if the BB-coefficient immediately its *left* (small circle indicated by  $\downarrow$  in Fig. 5) is defined as the weighted average of the BB-coefficients marked as bullets with the weights indicated above. The *right* circled BB-coefficient is defined by the mirrored formula.



Figure 5: Symmetric rule of  $C^2$  join.

### 2.3. The structure of the guide surface: a map of total degree $d = 6$

In this section, we define maps  $\mathbf{b}^\Delta$  consisting of  $n$  pieces total degree  $d$ . When initialized to serve as a guide surface over the  $n$ -sided region, we will denote the piecewise  $C^1$  map as  $\mathbf{g}$ . The vertices of the  $n$  triangular domain pieces will correspond to mid-edges of the  $n$ -sided region.

The domain of the map  $\mathbf{b}^\Delta$  of total degree  $d$  is a regular  $n$ -gon  $D$  composed of  $n$  equal triangles with a common vertex  $\mathbf{O}$  at the origin. Fig. 6a shows one such triangle with sides defined by  $l_i = 0$ ,  $i = 0, 1, 2$ . Each linear function  $l_i$  is equal to 1 at the vertex opposite to  $l_i = 0$ . On the triangle we define a map  $\mathbf{b}$  of total degree  $d$  in Bernstein-Bézier form as

$$\mathbf{b} := \sum_{i+j+k=d} \mathbf{b}_{ijk} B_{ijk}^d, \quad i, j, k \geq 0, \quad B_{ijk}^d := \binom{d}{ijk} l_0^i l_1^j l_2^k. \quad (1)$$

Fig. 6b labels the BB-coefficients rotationally symmetric. In the following, we reserve the – superscript  $s$  to enumerate sectors  $s \in \{0, 1, \dots, n-1\}$  and the – superscript  $r$  for refinement levels  $r \in \{0, 1, \dots\}$ .

Patches  $\mathbf{b}^s$  and  $\mathbf{b}^{s+1}$  (modulo  $n$ ) on adjacent sectors join across the shared *sector boundary*

$$C^0 \text{ if } \mathbf{b}_{d-i,i,0}^{s+1} := \mathbf{b}_{d-i,0,i}^s, \quad i=0, \dots, d \quad \mathbf{c} := \cos \frac{2\pi}{n}, \quad w_0 := -1, \quad w_1 := 2\mathbf{c}, \quad w_2 := 2(1-\mathbf{c}), \quad (2)$$

$$C^1 \text{ if } \mathbf{b}_{d-i,i-1,1}^{s+1} := w_0 \mathbf{b}_{d-i,1,i-1}^s + w_1 \mathbf{b}_{d-i,0,i}^s + w_2 \mathbf{b}_{d-i+1,0,i-1}^s, \quad i=1, \dots, d \quad (3)$$

$$C^2 \text{ if } \mathbf{b}_{d-i,i-2,2}^{s+1} := w_0^2 \mathbf{b}_{d-i,2,i-2}^s + 2w_0 w_1 \mathbf{b}_{d-i,1,i-1}^s + w_1^2 \mathbf{b}_{d-i,0,i}^s + 2w_0 w_2 \mathbf{b}_{d-i+1,1,i-2}^s + 2w_1 w_2 \mathbf{b}_{d-i+1,0,i-1}^s + w_2^2 \mathbf{b}_{d-i+2,0,i-2}^s, \quad i=2, \dots, d. \quad (4)$$

$$C^3 \text{ if } \mathbf{b}_{d-i,i-3,3}^{s+1} := w_0^3 \mathbf{b}_{d-i,3,i-3}^s + 3w_0^2 w_1 \mathbf{b}_{d-i,2,i-2}^s + 3w_0 w_1^2 \mathbf{b}_{d-i,1,i-1}^s + w_1^3 \mathbf{b}_{d-i,0,i}^s + 3w_0^2 w_2 \mathbf{b}_{d-i+1,2,i-3}^s + 6w_0 w_1 w_2 \mathbf{b}_{d-i+1,1,i-2}^s + 3w_1^2 w_2 \mathbf{b}_{d-i+1,0,i-1}^s + 3w_0 w_2^2 \mathbf{b}_{d-i+2,1,i-3}^s + 3w_1 w_2^2 \mathbf{b}_{d-i+2,0,i-2}^s + w_2^3 \mathbf{b}_{d-i+3,0,i-3}^s, \quad i=3, \dots, d. \quad (5)$$

The ten BB-coefficients  $\mathbf{b}_{ijk}^0$  (indicated as red bullets in Fig. 6) define a cubic expansion  $\mathbf{q}$  at the central point  $\mathbf{b}_{d00}^0$ . This local expansion is propagated to the neighboring sectors by repeatedly enforcing Eq. (2) for  $i = 0, 1, 2, 3$ , Eq. (3) for  $i = 1, 2, 3$  and Eq. (4) for  $i = 2, 3$  and Eq. (5) for  $i = 3$ . That is, the 10  $\mathbf{b}_{ijk}^0$  define a unique cubic expansion of the  $C^1$  map  $\mathbf{b}^\Delta$  at  $\mathbf{b}_{d00}^0$ .

With the cubic expansion fixed, the  $C^1$  constraints (3) can be rewritten as

$$\mathbf{b}_{d-i,0,i}^s := \frac{1}{2\mathbf{c}} (\mathbf{b}_{d-i,1,i-1}^s + \mathbf{b}_{d-i,i-1,1}^{s+1}) + (1 - \frac{1}{\mathbf{c}}) \mathbf{b}_{d-i+1,0,i-1}^s, \quad i = 4, \dots, d. \quad (3')$$

leaving the BB-coefficients

$$\mathbf{b}_{213}^s, \mathbf{b}_{231}^{s+1}, \mathbf{b}_{114}^s, \mathbf{b}_{141}^{s+1}, \mathbf{b}_{015}^s, \mathbf{b}_{051}^{s+1}$$

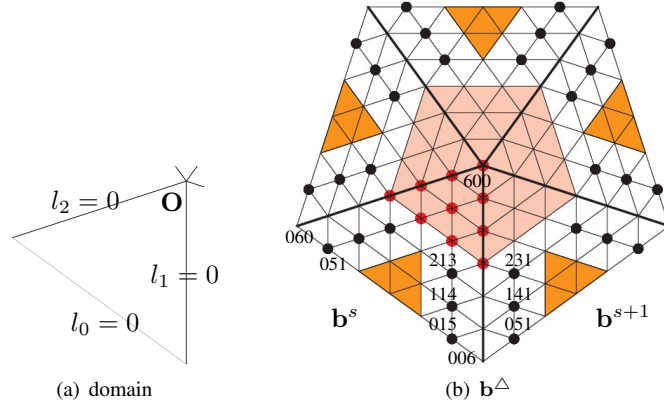


Figure 6: (a) Domain of total degree  $d$  map. (b) The  $n = 5$  sectors of the  $C^1$  map  $\mathbf{b}^\Delta$  of total degree 6. The coefficients of the cubic expansion at the center are underlaid light red. BB-coefficients unrestricted after enforcing the  $C^1$  constraints are marked as black and red bullets. The gold underlaid BB-coefficients do not affect  $C^1$  continuity between sectors.

of  $\mathbf{b}^\Delta$  unrestricted by the  $C^1$  continuity constraints (see Fig. 6b; coefficients unrestricted due to their distances from the sector boundary are underlaid gold).

The resulting map  $\mathbf{b}^\Delta$  is a piecewise  $C^1$  map of total degree 6 with a unique cubic expansion at the central point and  $12n + 10$  free parameters: 10 defining the cubic expansion,  $6n$  marked as black bullets and  $6n$  gold-underlaid in Fig. 6.

### 3. Bi-6 guided subdivision

#### 3.1. Characteristic parameterizations $\chi_\sigma$ and $\tilde{\chi}_\sigma$

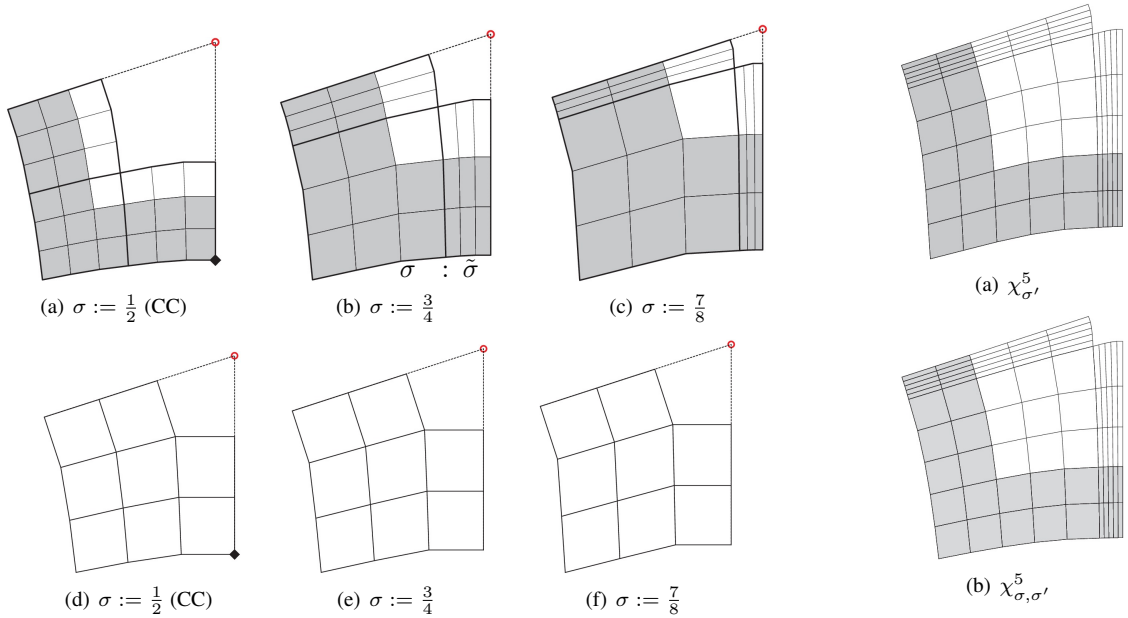


Figure 7: Top row:  $\chi_\sigma$ ; bottom row:  $\tilde{\chi}_\sigma$ .

Figure 8: Construction of  $\chi_{\sigma, \sigma'}$ .

The subdominant eigenvalue of bi-3 adjustable speed subdivision [13] with 'speed' parameter  $\sigma$  is

$$\lambda_\sigma := \frac{\tilde{\sigma}}{2}((1+c)\sigma^2 + 2\tilde{\sigma} + \sigma \sqrt{(1+c)((1+c)\sigma^2 + 4\tilde{\sigma}}), \quad \tilde{\sigma} := 1 - \sigma, \quad 0 < \sigma < 1. \quad (6)$$

When  $\sigma := \frac{1}{2}$  then  $\lambda_\sigma$  is the subdominant eigenvalue of Catmull-Clark subdivision,  $\sigma > \frac{1}{2}$  yields faster and  $\sigma < \frac{1}{2}$  yields slower contraction. Already for  $\sigma \approx \frac{1}{2}$ , analogous to Catmull-Clark subdivision, the subdivision surfaces of [13] do not qualify for high-end design; and the shape deteriorates with increasing  $\sigma$ .

Fig. 7<sup>top</sup> displays several characteristic maps  $\chi_\sigma$  for  $n = 5$  and one sector. Fig. 7<sup>bottom</sup> displays the corresponding characteristic tensor-borders  $\tilde{\chi}_\sigma$  of degree 3 and depth 2. In the classical analysis of Catmull-Clark subdivision these tensor-borders are hidden since the maps  $\chi_\sigma$  contain the key analytic information. For the new subdivision these  $C^2$  prolongations are in the forefront, since they facilitate sampling the guide with increasing speed (see Fig. 8b), an essential feature of the new approach. The gray underlaid BB-coefficients of  $\chi_\sigma$  are the result of splitting  $\tilde{\chi}_\sigma$  in the ratio  $\sigma : 1 - \sigma$  (see Fig. 7b). We consider normalized maps and tensor-borders where the corner BB-coefficients (marked as diamonds in Fig. 7a,d) are at the distance 1 from the red center. While different  $\sigma$  result in different maps  $\chi_\sigma$ , the corresponding tensor borders  $\tilde{\chi}_\sigma$  although different, look alike. This allows constructing well-behaved bi-5 transition parameterizations  $\chi_{\sigma,\sigma'}^5$  from one speed parameter to another.

Fig. 8 shows the transition for  $(\sigma, \sigma') := (\frac{1}{2}, \frac{7}{8})$ : in Fig. 8a  $\chi_{\sigma'}$  is degree-raised to degree bi-5 and named  $\chi_\sigma^5$ . Fig. 8b shows the gray-underlaid BB-coefficients in (a) replaced by the tensor-border  $\tilde{\chi}_\sigma$  degree-raised to bi-5 and split in the ratio  $\sigma' : 1 - \sigma'$  (light-gray underlaid BB-coefficients). This yields the map  $\chi_{\sigma,\sigma'}^5$ . (We note that  $\chi_{\sigma,\sigma}^5$  coincides with  $\chi_\sigma$ )

### 3.2. Guide initialization

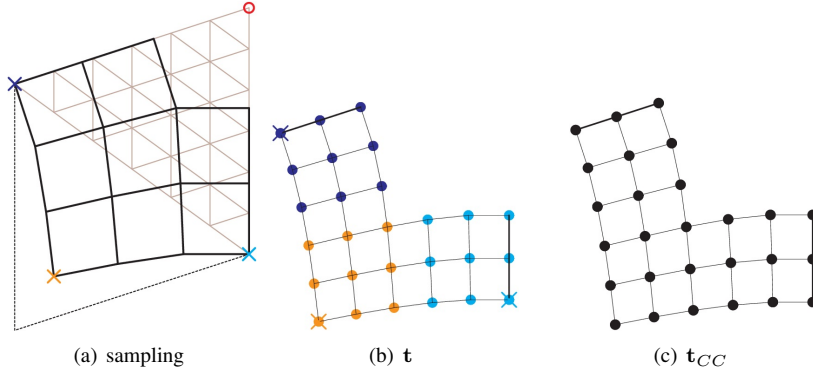


Figure 9: (a) Map  $\tilde{\chi}_{\frac{1}{2}}$  for sampling the guide  $\mathbf{g}$ ; (b) tensor-border  $\mathbf{t}$ . (c) tensor-border  $\mathbf{t}_{CC}$ .

As in Fig. 4d, the tensor-border  $\mathbf{t}$  in Fig. 9b is assembled from corner jets  $[\mathbf{g} \circ \tilde{\chi}_{\frac{1}{2}}]^5$  that sample  $\mathbf{g}$  in each sector at the locations marked as crosses in Fig. 9a. We set the central BB-coefficient  $\mathbf{b}_{600}^6$  as

$$\text{if } n > 4, \quad \frac{n}{n+5} \mathbf{c}_7^0 + \sum_{k=0}^{n-1} (\gamma_5 \mathbf{c}_5^k + \gamma_6 \mathbf{c}_6^k), \quad \gamma_5 := \frac{1}{n(n+5)}, \quad \gamma_6 := 4\gamma_5, \quad (7)$$

$$\text{if } n = 3, \quad (1 - 3\gamma_5 - 3\gamma_6) \mathbf{c}_7^0 + \sum_{k=0}^2 (\gamma_5 \mathbf{c}_5^k + \gamma_6 \mathbf{c}_6^k), \quad \gamma_5 := \frac{5}{96}, \quad \gamma_6 := \frac{1}{6}, \quad (8)$$

i.e. as the extraordinary point of Catmull-Clark subdivision except for a small perturbation to improve shape when  $n = 3$ . The remaining  $12n + 9$  free parameters are fixed by minimizing the sum of squared distances between the BB-coefficients of the sampled tensor-border  $\mathbf{t}$  and the corresponding BB-coefficients of the input tensor-border  $\mathbf{t}_{CC}$ .

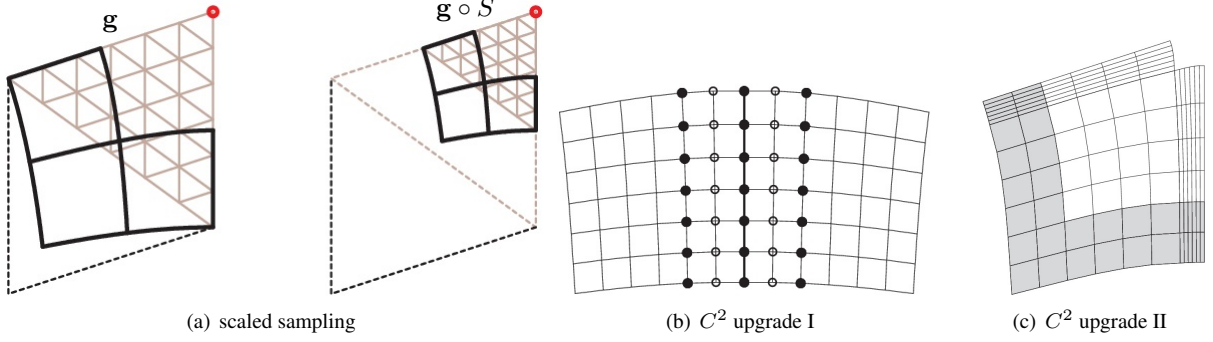


Figure 10: (a) Sampling the guide  $\mathbf{g}$  with  $\chi$ ; (b)  $C^2$  correction between sectors; (c)  $C^2$  upgrade between rings.

### 3.3. Construction of $C^2$ guided bi-6 rings

The bi-6 patches  $\mathbf{p}$  (see Fig. 4c) are assembled from the corner jets

$$[\mathbf{g} \circ (\mu\chi^5)]^6, \quad \text{for } 0 < \mu < 1.$$

Adjacent sectors are automatically  $C^1$ -connected and are  $C^2$ -connected by applying C2-rule (see Fig. 10b). Computing  $[\mathbf{g} \circ (\mu\chi_{\sigma, \sigma'}^5)]$  is equivalent to linearly mapping  $S : D \rightarrow \mu D$  (scaling of  $D$  with respect to red origin in Fig. 10a) and sampling  $(\mathbf{g} \circ S) \circ \chi_{\sigma, \sigma'}^5$ . DeCasteljau's algorithm (see Appendix) yields the BB-coefficients of  $\mathbf{g} \circ S$  as the affine combinations of BB-coefficients of  $\mathbf{g}$ . Due to combinatorial symmetry it suffices to pre-compute de Casteljau's refinement only for the 28 coefficients of one sector, for symbolic  $\mu$ . This is stored as a  $28 \times 28$  matrix. For fixed pairs  $(\sigma_{r-1}, \sigma_r)$  the sampled sectors are pre-computed as affine combinations of the BB-coefficients of  $\mathbf{g}$ . Again it suffices to pre-compute one sector and for the default speed sequence, it suffices to pre-compute two pairs.

With superscripts denoting refinement level  $l$  (scaling) of the ring, we have the following

#### Bi-6 Algorithm:

- Choose the maximal anticipated refinement level  $\ell$  and the

$$\text{sequence of speeds } (\sigma_0, \boldsymbol{\sigma}) := \left(\frac{1}{2}, \sigma_1, \sigma_2, \dots, \sigma_\ell\right).$$

Since the incoming tensor-border data prescribe  $\sigma_0 := \frac{1}{2}$ , we only list  $\boldsymbol{\sigma}$  in the remainder.

- Initialize  $\mathbf{g}^0 := \mathbf{g}$ .
- For  $r = 0, \dots, \ell - 1$ 
  - Per sector, apply the pre-computed de Casteljau split with  $\mu := \lambda_{\sigma_r}$  to obtain the BB-coefficients of  $\mathbf{g}^r$  from  $\mathbf{g}^{r-1}$ .
  - Sample  $\mathbf{g}^r$  with the pre-computed  $(\sigma_r, \sigma_{r+1})$  sampling rules to initialize the ring  $\mathbf{x}^r$ .
  - Apply the C2-rule correction.
  - $C^2$ -connect the consecutive rings  $\mathbf{x}^{r-1}$  and  $\mathbf{x}^r$  via  $C^2$  prolongation of the split ring  $\mathbf{x}^{r-1}$  (setting the gray-underlaid BB-coefficients of  $\mathbf{x}^r$  in Fig. 10c; if  $r = 0$  these coefficients stem from the degree-raised and split tensor-border  $\mathbf{t}_{CC}$ ).

## 4. Subdivision eigen-structure

Since the Bernstein polynomials  $B_{0jk}^d := \binom{d}{0jk}_{l_1 l_2}^j l_2^k$  are homogeneous of degree  $d$ ,  $B_{0jk}^d(\lambda x) = \lambda^d B_{0jk}^d(x)$  for any  $\lambda$  and this homogeneity is not affected by constraints (2-5). If we set one unconstrained BB-coefficient to 1 and the others to 0, the resulting  $\mathbf{g}$  is homogeneous in all sectors. We can so decompose the guide  $\mathbf{g}$  into homogeneous functions:

- 10 functions corresponding to cubic expansion: the function 1, two linear functions of degree 1, three of degree 2 and four of degree 3.
- $6n$  functions that are non-zero on two adjacent sectors:  $2n$  of degree 4,  $2n$  of degree 5 and  $2n$  of degree 6.
- $6n$  functions ( $n$  groups of 6) that are non-zero only in one sector:  $B_{022}^4$  of degree 4,  $B_{032}^5, B_{023}^5$  of degree 5,  $B_{042}^6, B_{033}^6, B_{024}^6$  of degree 6.

Assume  $\mathbf{x}^0$  is the first ring generated with a sequence of only fixed  $\sigma$ . Denote by  $\mathbf{x}_{d,p}^r$  the  $r$ th ring obtained by applying the Bi-6 Algorithm to the  $p$ th homogeneous function of degree  $d$  of the decomposition of the guide. Then  $\mathbf{x}_{d,p}^r = (\lambda_\sigma^d)^r \mathbf{x}_{d,p}^0$ . (This implies that we can, analogous to [14], pre-compute the initial  $12n + 10$  eigen-rings  $\mathbf{x}_{d,p}^0$  and compute eigen-functions  $\mathbf{x}_{d,p}^r$  simply by scaling by  $(\lambda_\sigma^d)^r$ . However, due to fast contraction this hardly makes sense in practice.) A linear combination of the two homogeneous eigen-functions of degree 1 re-produce  $\chi_\sigma$ ; and  $\chi_\sigma$  is injective according to [13]. Since the linear eigen-functions generate (by construction) the quadratic eigen-functions and the subsubdominant eigenvalue is the square of the subdominant eigenvalue, the bi-6 subdivision surfaces are  $C^2$  at the extraordinary point (see [15]).

## 5. The central cap

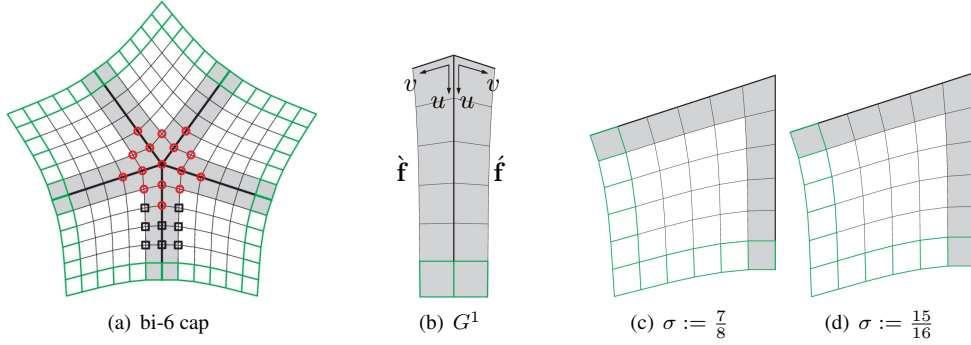


Figure 11: (a) The structure of bi-6 cap. (b)  $G^1$  constraints. (c,d) The parameterizations  $\tau$ . The reparameterizations  $\tau$  for different  $\sigma$  are visually similar. But the 'wrong'  $\sigma$  results in tiny caps of low quality.

The central cap is formed by  $n$   $G^1$ -connected bi-6 patches that join  $C^1$  with the last ring  $\mathbf{x}^{\ell-1}$ . The  $C^1$  prolongation of  $\mathbf{x}^{\ell-1}$  defines the cap's BB-coefficients that are green underlaid in Fig. 11a. The light-gray underlaid BB-coefficients enforce unbiased  $G^1$  constraints between the adjacent patches (see Fig. 11b):

$$\partial \hat{\mathbf{f}}_v + \partial \hat{\mathbf{f}}_u - 2c(1-u)^2 \partial \hat{\mathbf{f}}_a = 0. \quad (9)$$

*Planar reparameterization  $\tau$ .* First, for (each) fixed  $\sigma$  we construct a symmetric planar parameterization  $\tau$  (Fig. 11c shows one sector when  $n = 5$ ) so that

- adjacent sectors of  $\tau$  satisfy the constraints (9);
- the BB-coefficients that are green underlaid in Fig. 11c stem from  $\tilde{\chi}_\sigma$  degree-raised to bi-6;
- $\tau$  is rotationally symmetric and symmetric with respect to the sector diagonal.

Then  $\tau$  has 14 free parameters that, collected in the set  $\Gamma$ , are chosen to minimize

$$\min_{\Gamma} \sum_{s=0}^{n-1,*} \mathcal{F}_5(\tau^s), \quad \mathcal{F}_k f := \int_0^1 \int_0^1 \sum_{\substack{i+j=k \\ i,j \geq 0}} \frac{k!}{i!j!} (\partial_s^i \partial_t^j f)^2 ds dt, \quad (10)$$

where \* indicates that the sum is over both coordinates of  $\tau$ . Due to symmetry, this minimization is local to one sector.

The subsequent calculations work with symbolic coefficients of  $\mathbf{g}$  to obtain a general formula in terms of any geometric realization of the guide  $\mathbf{g}$ :

- Assemble a map  $\mathbf{h}$  from corner jets  $[\mathbf{g} \circ \tau]$  as in Fig. 4c. (The **red** BB-coefficients of  $\mathbf{h}$  are then consistent with the  $G^1$  constraints (9)).
- Replace the **green** underlaid BB-coefficients of  $\mathbf{h}$  by the  $C^1$  prolongation of the bi-6 patches constructed from the corner jets  $[\mathbf{g} \circ (\lambda_\sigma^{-1} \chi_\sigma)]$  (see Fig. 4c).
- Enforce the  $G^1$  constraints (9) along the sector separators by expressing the eight BB-coefficients, marked as squares in Fig. 11a, as affine combinations of the **green** tensor-border, the quadratic expansion and the four free BB-coefficients.
- Set the four free BB-coefficients by minimizing the sum of squared distances between the eight BB-coefficients marked as squares and their counterparts in  $\mathbf{h}$ .

The resulting formulas are applied to  $\mathbf{g}^l$  and  $C^1$  extension of  $\mathbf{x}^{l-1}$ . Since the **red** BB-coefficients represent a reparameterized quadratic expansion of  $\mathbf{g}^l$  at the central point, the  $G^1$  cap has well-defined curvature at the extraordinary point.

## 6. Examples and discussion

In the following, when the layout of the polynomial pieces is displayed, the surrounding bi-3 ring is colored **green**.

$$\text{For } n > 4, \text{ the default speed sequence is } \ell := 2, \quad \boldsymbol{\sigma} := (\sigma_1, \sigma_2) := \left(\frac{7}{8}, \frac{15}{16}\right).$$

This yields a central cap smaller than 8 CC-refinements. Setting  $\sigma_1 := \frac{15}{16}$  typically yields good quality but results in minor flaws in some extreme configurations. Similarly, setting  $\sigma_2 := \frac{31}{32}$  yields a (minutely) worse highlight line distribution.

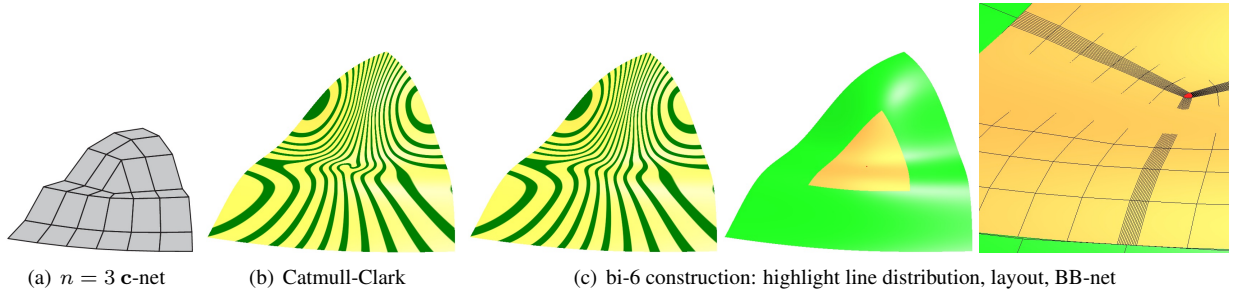


Figure 12: Valence  $n = 3$  and choice  $\ell = 1, \sigma_1 = \frac{31}{32}$ , central cap is **red**.

The case  $n = 3$  is special:  $\boldsymbol{\sigma} := (\frac{31}{32})$  yields high quality 3-sided surface and a tiny cap, see Fig. 12. Juxtaposition of highlight lines in Fig. 12b,c demonstrates improved shape over Catmull-Clark subdivision.

Fig. 14 elaborates on the construction of local features exploiting the well-known fact that  $C^2$  B-splines of degree bi-6 have many BB-coefficients unconstrained by  $C^2$  requirements. E.g. splitting a patch non-uniformly into  $3 \times 3$  subpatches as in Fig. 14b leaves free the BB-coefficients marked as black bullets. These are lifted up to form a cross while the circled BB-coefficients enforce the  $C^2$  connection. An analogous lifting up yields the embossing of Fig. 14c.

Although the central  $G^1$  cap construction assumes that the cap is so tiny that no more refinements are needed for geometry or analysis (spot the red cap in Fig. 13b!), the shape requirements are high in practice: the central cap should not be noticeable in the highlight line distribution Fig. 13c, even under magnification Fig. 13f. The  $C^2$  parameterization means that adding geometric details to the surface (see Fig. 13h) is supported by standard knot insertion (which has well-known benefits and limitations such as a preference for aligning finer geometric details with parameter lines and not diagonal to them).

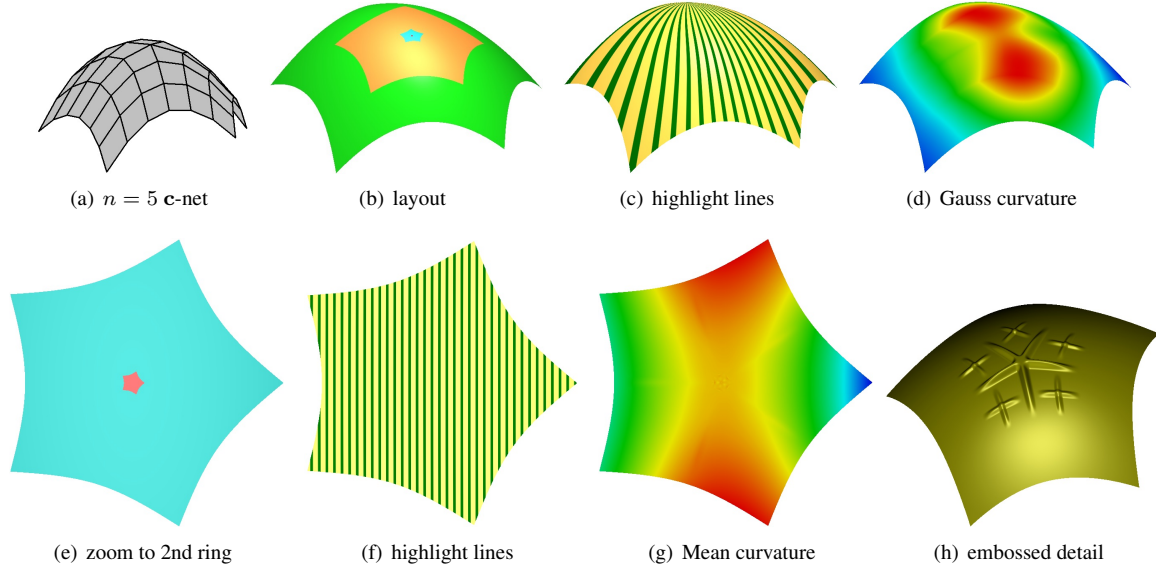


Figure 13: Convex bi-6 surface for  $\ell = 2$ ,  $\sigma := (\frac{7}{8}, \frac{15}{16})$  with red central cap. (The  $\mathbf{c}$ -net is the control net of the characteristic map of Catmull-Clark subdivision projected onto a paraboloid  $z = x^2 + 0.6y^2$ .) The second and innermost ring  $\mathbf{x}^1$  is blue in (b,e). (f) and (g) display correspondingly the highlight lights and mean curvature of zoom in (e). (h) embossing the details exploiting a refinability.

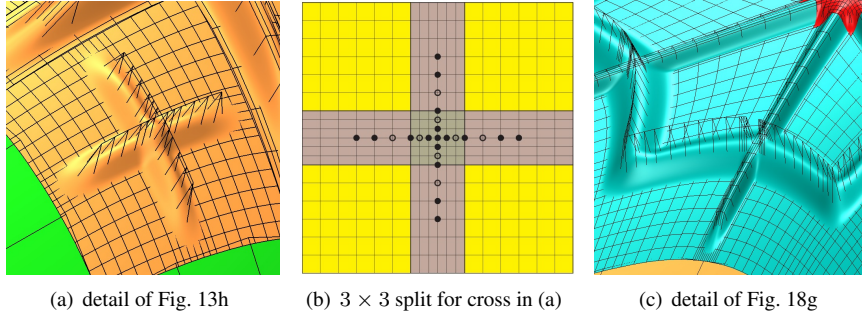


Figure 14: (a) Embossed cross from Fig. 13h with BB-net superimposed. (b) BB-coefficients marked as  $\bullet$  are not constrained by  $C^2$  requirements.

Fig. 15e demonstrates that the default sequence  $\sigma := (\frac{7}{8}, \frac{15}{16})$  works well also for challenging inputs. A similar bi-5 construction requires at least three guided rings to avoid shape deficiencies (see the arrow in Fig. 15d for a construction with the same speed sequence but degree bi-5). Fig. 15g,h further illustrate this trade-off between permissible contraction speed and the degree: if we reduce the sequence to  $\ell := 1$  and  $\sigma := (\frac{31}{32})$  the bi-6 surface construction exhibits flaws (see arrow in Fig. 15g) but a similar construction of degree bi-7 can handle also the extreme speed. The presented algorithm with the default choice appears to be the best trade-off in practice of surface degree and number of patches.

Fig. 16 places a complex surface under the microscope, comparing again, for default speed sequence, the presented bi-6 construction with a similar bi-5 construction. The bi-5 ring  $\mathbf{x}^0$  is acceptable, but the second bi-5 ring  $\mathbf{x}^1$  in Fig. 16d contracts too fast for the data.

Fig. 17 underscores the resilience of the default choice of  $\sigma$  also for a complex higher-order input  $\mathbf{c}$ -net with  $n = 7$ .

Fig. 18 interrogates the converse case: rather than increasing  $\sigma$ , we decrease its second entry to slow contraction Fig. 18e. The highlight line distribution for Fig. 18e and  $\sigma_2 := \frac{7}{8}$  is the same as for Fig. 18c and  $\sigma_2 := \frac{15}{16}$  and is shown in Fig. 18d. Zooming in (Fig. 18f,g), we see that the default surface quickly approaches the characteristic configuration of adjustable speed subdivision [13] so that local editing of the second ring has predictable results even

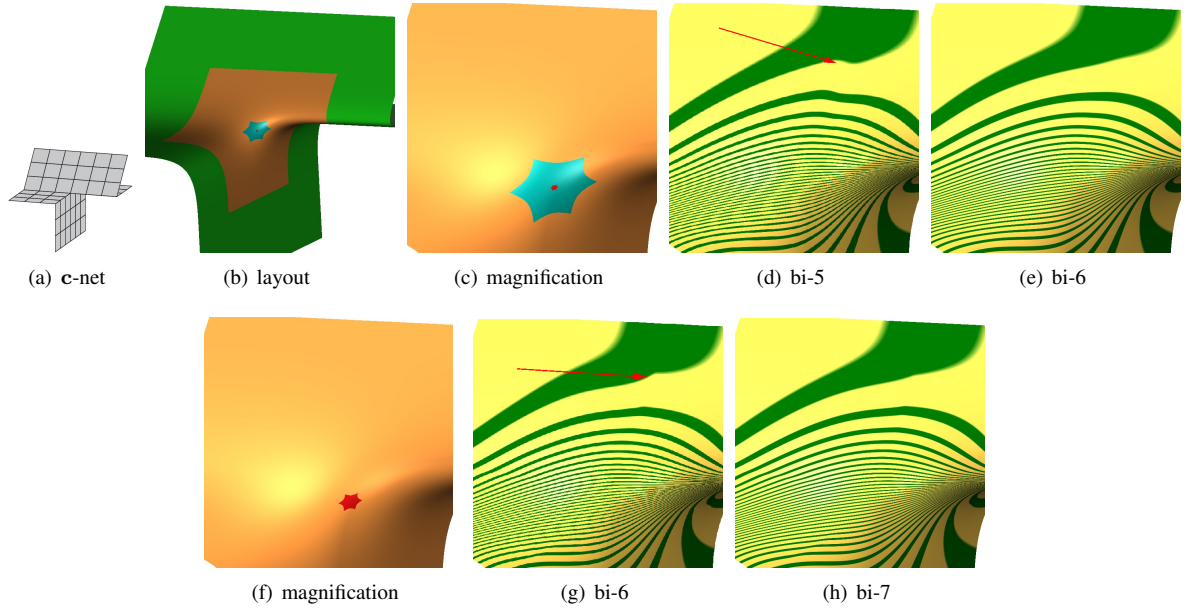


Figure 15: Comparison of various surfaces from (a)  $n = 6$  c-net. Top row:  $\ell := 2, \sigma_1 = \frac{7}{8}, \sigma_2 = \frac{15}{16}$ . Bottom row:  $\ell = 1, \sigma_1 = \frac{31}{32}$ . (d) is shared for (c) and (e).

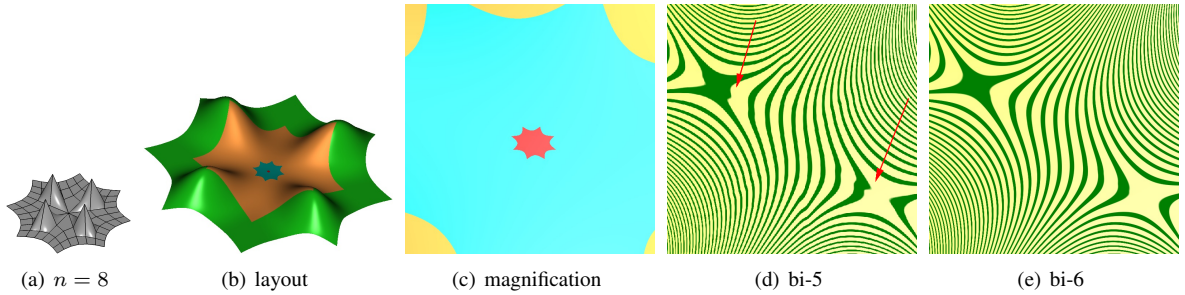


Figure 16: The surfaces from (a)  $n = 8$  c-net for the default choice  $\ell = 2, \sigma := (\frac{7}{8}, \frac{15}{16})$ . (c) innermost ring + central cap.

for unusual inputs.

## 7. Conclusion

Almost everywhere parametrically  $C^2$  free-form surfaces leverage the theory of subdivision towards the practical end of generating surfaces with few pieces and, except for tiny caps,  $C^2$  transitions between patches. A ‘class A’ highlight line distribution is obtained by reference to a guide shape as originally proposed in [10]. The shape improvements are major compared to Catmull-Clark subdivision. The larger stencil appears to be the unavoidable cost for obtaining better highlight line distributions; there is no indication to date that small-stencil subdivision can produce ‘class A’ highlight line distributions. The advantage over earlier guided constructions lies in the more efficient and analysis-friendly structure.

A number of variants are possible and should be explored: guided subdivision surface rings of degree bi-5 and bi-7 can be derived akin to the present algorithm and also lower degree with more patches may ultimately yield good results.

*Acknowledgements.* This work was supported in part by NSF grant CCF-1117695, DARPA HR00111720031 and NIH R01 LM011300-01.

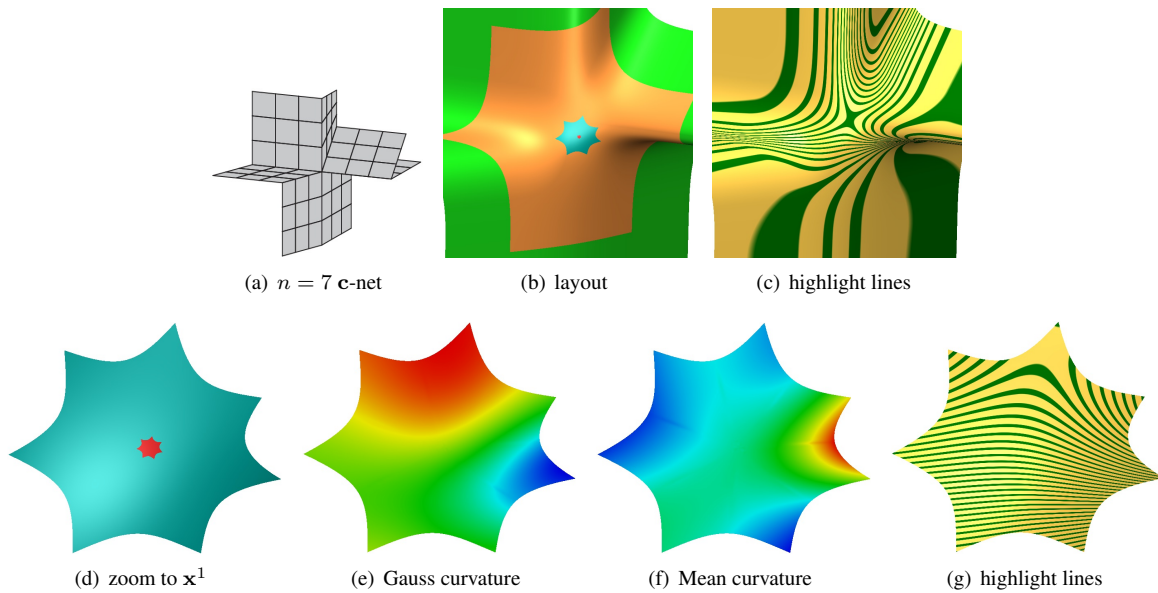


Figure 17: The surfaces from (a)  $n = 7$  c-net for a default choice  $\ell = 2$ ,  $\sigma_1 := \frac{7}{8}$ ,  $\sigma_2 := \frac{15}{16}$ .

- [1] G. Farin, *Curves and Surfaces for Computer Aided Geometric Design: A Practical Guide*, Academic Press, San Diego, 2002.
- [2] J. Peters, Geometric continuity, in: *Handbook of Computer Aided Geometric Design*, Elsevier, 2002, pp. 193–229.
- [3] T. Nguyen, K. Karčiauskas, J. Peters, A comparative study of several classical, discrete differential and isogeometric methods for solving Poisson’s equation on the disk, *Axioms* 3 (2) (2014) 280–299.
- [4] K. Karčiauskas, T. Nguyen, J. Peters, Generalizing bicubic splines for modelling and IGA with irregular layout, *Computer Aided Design* 70 (2016) 23–35.
- [5] B. Mourrain, R. Vidunas, N. Villamizar, Dimension and bases for geometrically continuous splines on surfaces of arbitrary topology, *Computer Aided Geometric Design* 45 (2016) 108–133.
- [6] M. Kapl, G. Sangalli, T. Takacs, Dimension and basis construction for analysis-suitable  $G^1$  two-patch parameterizations, *Computer Aided Geometric Design* 52 (2017) 75–89.
- [7] M. Bercovier, T. Matskewich, *Smooth Bzier Surfaces over Unstructured Quadrilateral Meshes*, Springer Verlag, 2017.
- [8] D. Grossier, J. Peters, Matched  $G^k$ -constructions always yield  $C^k$ -continuous isogeometric elements, *Computer Aided Geometric Design* 34 (2015) 67–72.
- [9] K. Karčiauskas, J. Peters, Refinable  $G^1$  functions on  $G^1$  free-form surfaces, *Computer Aided Geometric Design* 54 (2017) 61–73.
- [10] K. Karčiauskas, J. Peters, Concentric tessellation maps and curvature continuous guided surfaces, *Computer Aided Geometric Design* 24 (2) (2007) 99–111.
- [11] K.-P. Beier, Y. Chen, Highlight-line algorithm for realtime surface-quality assessment, *Computer-Aided Design* 26 (4) (1994) 268–277.
- [12] H. Prautzsch, W. Boehm, M. Paluszny, *Bézier and B-spline techniques*, Springer Verlag, 2002.
- [13] K. Karčiauskas, J. Peters, Adjustable speed surface subdivision, *Computer Aided Geometric Design*. 26 (2009) 962–969.
- [14] J. Stam, Exact evaluation of Catmull-Clark subdivision surfaces at arbitrary parameter values, in: *Proceedings of the ACM Conference on Computer Graphics (SIGGRAPH-98)*, ACM Press, New York, 1998, pp. 395–404.
- [15] J. Peters, U. Reif, *Subdivision Surfaces*, Vol. 3 of *Geometry and Computing*, Springer-Verlag, New York, 2008.
- [16] J. Peters, Evaluation and approximate evaluation of the multivariate Bernstein-Bézier form on a regularly partitioned simplex, *Transactions of Mathematical Software* 20 (4) (1994) 460–480.

## Appendix: BB-coefficients of a scaled triangular domain

It is well known that if Bézier curve with BB-coefficients  $\mathbf{p}_i$ ,  $i = 0, \dots, d$  of degree  $d$  defined over unit interval  $[0..1]$  is restricted to subinterval  $[0..\lambda]$ , BB-coefficients  $\bar{\mathbf{p}}_i$  of restriction can be computed via formula

$$\bar{\mathbf{p}}_i := \sum_{k=0}^i B_k^i(\lambda) \mathbf{p}_k,$$

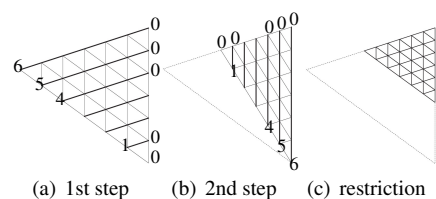


Figure 19: Domain restriction:  $D \rightarrow SD$ .

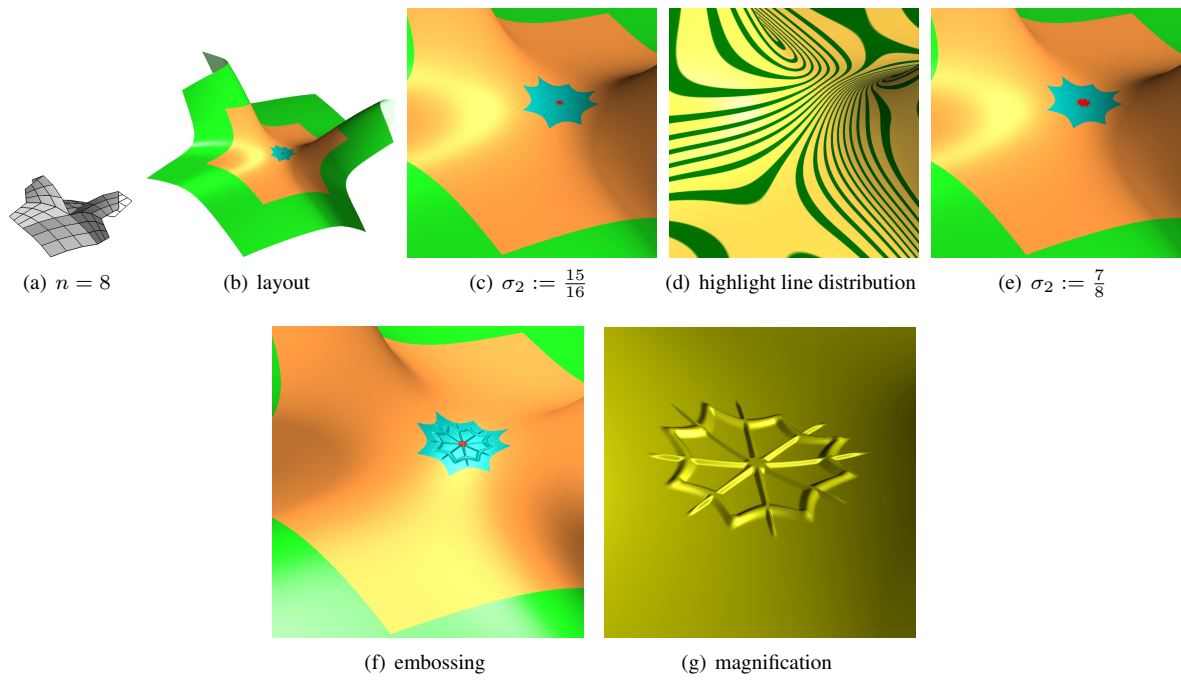


Figure 18: Surfaces from a c-net with  $n = 8$  using the default choice of contraction speed  $\sigma$  (except for (e) where  $\sigma_2 := \frac{7}{8}$ ).

where  $B_k^i$  are the Bernstein polynomials. Applying this formula first in one parameter and then in a second yields the BB-coefficients of the restriction to scaled triangular domain (see Fig. 19a,b and [16]).